Exploring the magnetic properties of cobalt-ferrite nanoparticles for the development of rare-earth-free permanent magnet

A. López-Ortega[‡*], E. Lottini[‡], C. de Julián Fernández[§] and C. Sangregorio[⊥*]

[‡]INSTM and Università degli Studi di Firenze, Sesto Fiorentino (Firenze), Italy.

[§]INSTM and CNR-IMEM, I-43124 Parma, Italy.

[⊥]INSTM and CNR-ICCOM, I-50019 Sesto Fiorentino (Firenze), Italy

ABSTRACT

We present for the first time an in-depth magnetic characterization of a family of monodisperse cobalt ferrite nanoparticles (NPs) with average size covering a broad range of particles sizes (from 4 to 60 nm), synthesized by thermal decomposition of metal-organic precursors. Metal precursors, surfactants and synthetic parameters were settled in order to fine tune the particle size, preserving in the meanwhile a narrow particle size distribution. The morphology of the family of cobalt ferrite NPs shows a size dependent behaviour, evolving from sphere to octahedrons for size larger than 20 nm and passing through a cubic habit for intermediate sizes. The evolution of the magnetic properties was studied as a function of the particle size and shape, particularly focusing on those determining the best performance as permanent magnet. While saturation and remnant magnetization increase monotonously with the size reaching a constant value above 20 nm, the coercive field exhibits a non-monotonic behaviour with two distinct maxima values for low and room temperature, respectively. In addition, we evaluated the $(BH)_{max}$ product, the figure of merit of permanent magnets, obtaining the maximum value ever reported in the literature for cobalt ferrite NPs (i.e., 2.1 MGOe (18 MJm^{-3}) for 40 nm NPs). This study allowed us to establish, at

least on the basis of the $(BH)_{max}$ product, the potentiality of cobalt ferrite nanoparticles in current permanent magnet technology.

KEYWORDS permanent magnet; magnetic anisotropy; size effect; cobalt ferrite, nanoparticles

INTRODUCTION

The risk of supply of some strategic technological raw materials, due to natural exhaustion, environmental or political restrictions, is pushing researchers from many countries to look for viable alternatives. A paradigmatic example is represented by permanent magnets. Permanent magnets are essential components in modern technologies, being employed in a huge number of large-scale and emerging applications, such as electronic devices, hard disks, automotive, wind turbines and hybrid – electric vehicles. Since their introduction in the late 60's, rare-earth (RE)-based compounds have quickly established as the strongest permanent magnets and nowadays they account for the largest production volume. [1,2] However, the high environmental impact of mining, refining and recycling of RE compounds may represent a serious drawback for the economic sustainability of their massive exploitation. Therefore, the scientific community is looking for new RE-free materials that, although they are not as strong permanent magnets as RE-based compounds, could at least replace them in a wide range of industrial applications, where lower performances are required.

In order to achieve this goal, the reduction of traditional magnetic materials, such as ferrites, to the nanoscale, has been proposed as a promising approach. The motivation relies on the prediction that a material is expected to reach its maximum coercive field, H_C, when entering the single domain size, where domain wall – reversal processes are no longer available. [3]

Moreover, at the nanoscale, size-dependent surface anisotropy, morphology controlled shape anisotropy and strain-induced magnetostriction contributions can add to the intrinsic anisotropy, improving the magnetic performances of the material. On the other hand, nanosized magnets suffer from H_C and remnant magnetization losses due to thermal demagnetization processes, an effect which becomes particularly relevant in the size range where marked enhancements in magnetic anisotropy are expected. Therefore, the development of novel permanent magnets based on nanoparticles, NPs, requires a careful control of the particle size to properly balance the single domain behaviour and thermally driven demagnetization effects.

One of the most promising materials to be investigated to this purpose is cobalt ferrite ($Co_xFe_{3-x}O_4$). Cobalt ferrite is a partially inverted mixed spinel ferrite, which has large cubic magnetocrystalline anisotropy, responsible for its large H_C, a high stability and easy manufacturing by cheap techniques. [4,5] All these properties, together with many other outstanding characteristics, such as magnetostriction [6] and large magneto-optical coefficients,[7] make cobalt ferrite extremely appealing for application in several technological fields including magnetic hyperthermia, [8,9] molecular imaging, [10] electronics, [11,12], spintronics, [13] supercapacitors [14] and catalysis. [15]

Nowadays, many different chemical approaches have been developed to reproducibly synthesize highly crystalline, monodisperse cobalt ferrite NPs with controlled size. [16–20] Among the others, the thermal decomposition approach appears as one of the most promising procedures to obtain highly structural (stoichiometric) and morphologically controlled NPs with exquisite crystallinity. [19,21,22] These achievements boosted a renewed interest towards the investigation of the physical properties of nanosized cobalt ferrite to conclusively establish the correlation between magnetic properties and stoichiometry, [5,23] particle size, [20,24–26] particle shape[19,27,28] or structural defects. [29,30] Despite of the number of publications which

each year continuously appear in the literature, to our knowledge, all these studies were limited to short particle sizes range and finite temperatures, leaving unconstrained the shape and stoichiometry.

In this work, for the first time we present an investigation on the magnetic properties of a series of cobalt ferrite NPs with size in a broad range (from 4 to 60 nm), narrow size distributions and controlled shape and stoichiometry. The evolution of the magnetic properties was studied as a function of the particles size and shape, with particular attention to those determining the best performance in view of a possible application for the realization of permanent magnets. In particular, we focused on the analysis of H_C, remnant magnetization, M_R, and the maximum energy product, $(BH)_{max}$. The latter represents the figure of merit of permanent magnets. We found that at low temperature 20 nm nanoparticles exhibit the best magnetic properties, while at room temperature the highest $(BH)_{max}$ is observed for nanoparticles with average size of ca. 40 nm. This is also the maximum $(BH)_{max}$ ever reported for randomly oriented cobalt ferrite NPs (2.1 MGOe (18 MJm^{-3})). Finally, the feasibility of the application of cobalt ferrites NPs in the realization of permanent magnet is discussed on the basis of the $(BH)_{max}$ product.

METHODS

Synthesis of cobalt ferrite NPs. The synthesis was carried out using standard airless procedures and commercially available reagents. Benzyl ether (Bz_2O, 99%), oleic acid (OA, 90%), oleylamine (ONH_2, >70%) iron(III) acetylacetonate ($Fe(acac)_3$, 99%), cobalt(II) acetylacetonate ($Co(acac)_2$, ≥ 99%), cobalt(II) chloride anhydrous ($CoCl_2$, ≥ 99%). All starting materials were purchased from Sigma-Aldrich and used without further purification. $CoCl_2$ anhydrous was stored inside a glove box.

Cobalt ferrite NPs were synthesized following a slightly modified procedure previously reported for the synthesis of iron-based cubic spinels, (MFe_2O_4), through thermal decomposition of organometallic compounds in high-boiling solvent containing oleic acid and oleylamine as stabilizing surfactants. The organic coating prevents direct contact between magnetic NPs and, thus, their aggregation. [21,31] In a typical synthesis 1 mmol of metal precursors ($Fe(acac)_3$ and $Co(acac)_2$ or $CoCl_2$) in a Fe:Co molar ratio of 2:1 were dissolved in a solution containing 4 mmol of OA, 4 mmol of ONH_2 and 50 mL of Bz_2O in a 100 mL three-neck round bottomed flask. Fe:Co precursors ratio has been chosen in order to obtain $Co_{0.6\text{-}0.7}Fe_{2.4\text{-}2.3}O_4$ stoichiometry. Initially, the mixture was degassed by bubbling N_2 at 120°C for 30 min and then it was heated up to the desired decomposition temperature setting heating rate, nucleation step and digestion time in order to control the final particle size. During the heating and digestion processes the mixture was exposed to a N_2 flow. Finally, the flask was removed from the heating mantle and allowed cooling down under inert atmosphere. All NPs were washed by several cycles of coagulation with ethanol, centrifugation at 5000 rpm, disposal of supernatant solution and re-dispersion in hexane.

Structural and Morphological Characterization. Transmission electron microscopy (TEM) images were obtained using a CM12 PHILIPS microscope with a LaB_6 filament operated at 100 kV. Helium Ion Microscopy (HIM) images were obtained using an Orion Plus Helium Ion Microscope from Carl Zeiss NTS operating at 35 kV. In both cases the NPs were dispersed in hexane and then placed dropwise onto a holey carbon supported grid. The particle size of the different samples and the standard deviation were obtained by calculating the number average by manually measuring the equivalent diameters/edge length of > 200 spherical/polyhedral particles from TEM micrographs. The determination of cobalt and iron concentrations in the samples was performed using a Rigaku ZSX Primus II X-ray fluorescence spectrometer (XRF). The Fe/Co ratios, evaluated from the intensity of Co and

Fe absorption peaks were found in the 3.3-4.0 range for the whole cobalt ferrite series, corroborating their similar stoichiometry (it corresponds to an x value of 0.6-0.7 i.e., $Co_{0.6-0.7}Fe_{2.4-2.3}O_4$). The structure of the NPs was investigated by X-ray powder diffraction (XRD) using a Bruker New D8 ADVANCE ECO diffractometer equipped with a Cu Kα radiation. The measurements were carried out in the range 20-70°, with a step size of 0.03° and a collection time of 1 s. Quantitative analysis of the XRD data was undertaken with a full pattern fitting procedure based on the Rietveld method using MAUD program.[32] Microstrain and crystal size were obtained using the isotropic size-strain model. [33]

Magnetic measurements. The magnetic properties of the NPs were measured on tightly randomly packed powder samples using a vibrating sample mode (VSM, Quantum Design PPMS) magnetometer with 90 kOe maximum field. The magnetization versus temperature measurements were performed in zero-field cooled (ZFC) and field cooled (FC) conditions with a 50 Oe probe field. The hysteresis loops were measured at increasing temperatures after FC in 50 kOe from 380 K to 5 K.

RESULTS AND DISCUSSION

A family of cobalt ferrite NPs with average size, d_{av}, from 4 to 60 nm and with a narrow size distribution was synthesized by thermal decomposition of metal-organic precursors in high-boiling point solvents. XRF analysis confirmed all the NPs have the same non-stoichiometric composition, $Co_{0.6-0.7}Fe_{2.4-2.3}O_4$, which has been demonstrated to correspond to the largest magnetic anisotropy for Co-doped ferrite NPs and have a magnetization saturation similar to that of bulk $CoFe_2O_4$. [5,34] In principle, these features should correspond to the best performance as permanent magnet. Figure 1a-g shows some representative bright field, low magnification TEM, images of the cobalt ferrite NPs and the corresponding particle size

histograms. The control of the NPs size was obtained by modifying the synthetic parameters related to the nucleation and growth processes (Table 1). The smaller NPs, with d_{av} from 4 to 11 nm, were synthesized by decomposition of $Fe(acac)_3$ and $Co(acac)_2$ using oleic acid, (OA) and oleylamine, (ONH_2), as surfactants, with the exception of 4 nm NPs. Indeed, the latter were synthesized using only ONH_2 as surfactant, following a slightly modified procedure already reported for the synthesis of MnO NPs.[31] This choice reduces the probability of the $Fe^{2+} \rightarrow Fe^{3+}$ oxidation, which, as recently demonstrated by Fantechi *et al*., [5] is significantly large for small non-stoichiometric cobalt ferrite NPs synthesized using OA and ONH_2 surfactants, providing, as final product cobalt doped maghemite (γ-Fe_2O_3). The control of d_{av} in this range was achieved by modifying the digestion time and the decomposition temperature (see Table 1). Low decomposition temperature (i.e., 210 ºC) leads to small NPs with an average diameter of 4(1) nm. It should be noted that at this decomposition temperature the digestion time must be larger than 300 min in order to obtain crystalline NPs. Increasing the decomposition temperature to 270 ºC, adding a 2 hours nucleation step at 210 ºC, and shortening the digestion time from 300 min to 30 min or 60 min, NPs with average diameter of 7(1) and 11(1) nm, respectively, were obtained. TEM images show that small NPs exhibit a spherical shape. All the size histograms obtained from TEM micrographs by evaluating the particle diameter, *d*, can be well fitted by a Gaussian distribution, showing unique size population with a narrow distribution of diameter (deviation < 20%).

Larger NPs with edge length from 20 to 60 nm (d_{av}) were synthesized using anhydrous $CoCl_2$ as cobalt precursor. Different particle sizes were obtained controlling the digestion time and heating rate and keeping the decomposition temperature constant. A fast heating rate (3 ºC/min) permitted the synthesis of 20 to 30 nm NPs. On the other hand, a slow heating rate (1 ºC/min) favoured the formation of larger NPs in the 40 to 60 nm range. For a given heating rate the particle size could be further tuned by varying the digestion time from 15 to 60

minutes. Interestingly, TEM images demonstrated that on increasing the NP size the shape evolves from sphere to octahedron, passing through an intermediate size around 20 nm, where spheres and cubes coexist. The formation of octahedral NPs at large size was confirmed by HIM, as shown in Figures 1h-i, where images of 20 and 40 nm NPs are shown. In Figure 1j the cubic, rhombohedral and hexagonal 2D projections along [100], [110] and [111] directions of a regular octahedron/truncated octahedron placed over (111) or (100) faces is shown together with the corresponding TEM images.[35] The particle size histograms for non-spherical NPs, also reported in Figure 1, are referred to the average edge length of cubes or octahedrons (l).

Theoretically, cubic spinel structures should generate a cubic crystal habit, reflecting the growth along the preferential <100> axes, but our experimental result suggests that with our synthetic procedure, spherical and octahedral shapes are the most favoured, depending on the size. For small NPs the dominant role of surface tension drives the nanocrystal growth towards a spherical shape, which corresponds to the smallest surface area. Conversely, when the particle size is increased, the change in the shape from spheres to octahedrons is due to the faster growth rate along the <100> directions with respect to <111>, being {111} lowest energy facets.[36] Interestingly, NP with size close to the threshold between the two morphologies (20 nm), where surface tension and preferential <100> directions growth are balanced, exhibit a cubic shape.

Figure 2a depicts the XRD patterns recorded for the family of cobalt ferrite NPs. All diffraction patterns show the formation of a single crystallographic phase, which can be indexed as the cubic structure of spinel oxides (JCPDS PDF #221086). The series of diffractograms reveals the expected gradual narrowing of the peaks associated with the increase of d_{av}. The crystal size, evaluated from the diffraction patterns are consistent with

those obtained from TEM images, indicating the growth of single crystal NPs and their high crystallinity. In addition, cell parameter and crystal strain were determined and are reported in Figure 2b. The cell parameter for the whole series of cobalt ferrite NPs is constant and close to 0.840 nm. This fact supports the similar stoichiometry of all the synthesized NPs, as indeed indicated by XRF analysis. However, this value is slightly larger than that reported for Co-doped maghemite NPs with similar stoichiometry [5] suggesting the stabilization, even at small size, of a pure cobalt doped magnetite phase (Fe_3O_4, Fe^{2+}/Fe^{3+} oxide) where oxidation of Fe^{2+} ions did not take place. The evaluated microstrain is highest at the smallest crystallite size and then it decreases on increasing d_{av} vanishing, in the resolution limit of our experimental device, for size ≥ 20 nm. Interestingly, the structural distortions disappear at the same size at which the morphology of the NPs changes, suggesting that finite-size and surface effects can induce surface strain and concomitant structural perturbations leading to preferential morphological structures.[37] These results demonstrate the intimate correlations between particle morphology, crystal structure and particle size existing at the nanoscale.

In order to evaluate the magnetic performance of the as prepared cobalt ferrite NPs, a deep analysis of their static magnetic properties was performed by standard magnetometric technique. At first, the temperature dependence of the magnetization was investigated after zero field cooling, (ZFC) and field cooling, (FC), procedures (see Fig. S1, Supporting Information). For all the samples the behaviour characteristic of an ensemble of single domain NPs is observed. NPs smaller than 20 nm present a clear transition to the superparamagnetic state on their magnetization vs. temperature curves and they are therefore unblocked at RT. Conversely, larger NPs are still in the blocked state at RT, as required for the realization of permanent magnets. Figure 3 reports the blocking temperature (T_B) estimated as the maximum of the ZFC curves, as a function of d_{av}. For samples comprising NPs whose thermal de-blocking requires a temperature higher than that experimentally

investigated, T_B was estimated from the hysteresis loops recorded at various temperatures, using the expression $H_C=H_C(0)[1-(T/T_B)]^{\beta}$ (see discussion below for data and details). [38–40] Interestingly, extending this procedure to smaller NPs provides T_B values that well match those extracted from ZFC magnetization curves, supporting the validity of this approach. As expected, T_B increases with d_{av} consistently with the classical description for superparamagnetism. [41]

Figure 4a displays the hysteresis loops recorded at low temperature (5K), and the main parameters extracted from the loops, i.e. coercive field, (H_C), saturation magnetization, (M_S) and reduced remnant magnetization, ($R = M_R/M_S$, where M_R is the remnant magnetization), are shown in Figure 4b-d, as a function of d_{av}. All loops exhibit the characteristic features expected for hard ferro- or ferri-magnetic materials, i.e. non-zero M_R and high H_C. A non-monotonous dependence of H_C with d_{av} is observed: initially, H_C increases till it reaches the maximum value of 16.7 kOe for d_{av} = 20 nm, followed by a fast abatement for larger d_{av}. A similar size dependence of H_C is retained at room temperature (Fig. 4 and Fig. S2) although some differences are observed: indeed, due to the increased relevance of thermal demagnetization processes, the irreversibility is observed only for sample with $d_{av} \geq 20$ nm and the maximum H_C value is decreased to 3 kOe and shifted to larger d_{av}, i.e. 40 nm. The non-monotonic H_C dependence at low temperature can result from a cross-over in the magnetization switching mode and/or a demagnetization shape-induced effect. In other words, initially, H_C increases with the size as expected for single domain NPs, where the magnetization reverses its orientation through a uniform coherent rotation of all the atomic spins. [19,42–44] However, according to micromagnetic theory, curling rotation becomes favoured with respect to the coherent reversal mode when the radius, r, of a particle surpasses a certain limit, called coherent radius, r_{coh}. For small spherical NPs $r_{coh} = 3.6055l_{ex}$, l_{ex} being the exchange length.[45,46] Using the intrinsic magnetic properties of bulk cobalt ferrite, namely

the exchange stiffness constant and spontaneous magnetization, [47] $l_{ex} \approx 5.35$ nm can be estimated from which $r_{coh} = 17$ nm. According to this value, cobalt ferrite NPs with size larger than ~ 35 nm should show a cross-over on the magnetization reversal process from coherent to incoherent mode (curling), decreasing H_C as the particle size is further increased. [47,48] Interestingly, this value matches the diagonal of 20 nm cubic NPs. On the other hand, a concomitant effect of the variation of the particle shape can also be envisaged for larger NPs. Indeed, NPs with small and intermediate size mostly have regular spherical or mixed spherical/cubic shapes. However, in larger NPs, where the octahedron emerges as the preferential crystal habit, the demagnetization fields are preferentially generated at the corners, regions where incoherent rotation modes can be generated more easily as the particle size is larger, leading to a decrease of H_C. [49] It should be noted that a change in the shape may also affect the total magnetic anisotropy of the NPs through the surface contribution. [19,44] However, in our case the high magneto-crystalline anisotropy of cobalt ferrite and the large particle size make this contribution negligible. Finally, we wish to stress that a non-monotonous behaviour at RT was previously observed in a similar range of particle sizes for cobalt ferrite NPs synthesized by various techniques and was ascribed to the magnetic single- to multi-domain transition.[20,24,29,50,51] However, we do believe that this behaviour originates from the combination of a cross-over on magnetic rotation and/or demagnetization shape-induced effect, which are responsible for the maximum at low temperature, and thermal fluctuation of the blocked moment across the anisotropy barrier. The latter, being more important for lower sizes and at higher temperatures, produces a shift to large particle size of the H_C maximum.[52]

On the other hand, M_S and R show the same trend both at low and RT, increasing with the average particle size up to 20 nm and then remaining roughly constant at larger size at M_S = 80-90 emu/g, R = 0.75-0.83 and M_S = 80-85 emu/g, R = 0.5 for low and RT, respectively.

Low temperature data are in good agreement with those theoretically expected for randomly oriented cobalt ferrite nanograins with cubic magnetic anisotropy [53,54], while the RT ones, due to thermal effects, show a more pronounced increase with size for both M_S and R. It deserves to be pointed out that 4 nm NPs present peculiar magnetic properties with respect to the rest of the series. At low temperature we observed a 25% reduction of Ms, while R is only 0.6. These results indicate that for d_{av} < 20nm the magnetic disorder induced by large structural strain deteriorates the magnetic properties. In addition, for very small NPs a symmetry change of the magnetic anisotropy from cubic to uniaxial may concur to lower R. [53,55,56]

In order to further investigate the magnetic properties of the series of samples, the effective magnetic anisotropy, (K_{eff}), was estimated from the temperature dependence of H_C. If the magnetic anisotropy is temperature-independent and the switching is driven by a coherent rotation, the effective cubic magnetic anisotropy can be expressed as $K_{eff} = H_C(0)M_S/0,64$, [57,58] where $H_C(0)$ is the anisotropy field. The latter can be experimentally obtained from the analysis of the temperature dependence of the coercive field, which must follow the expression $H_C=H_C(0)[1-(T/T_B)]^{\beta}$, where β is an exponential factor which is 0.5 or 0.77 for oriented or randomly oriented assembly of particles respectively.[39,40,59] In Figure 5 K_{eff} estimated from the hysteresis loops recorded at various temperature in the 5-380 K range and neglecting the contribution from unblocked NPs, is shown. K_{eff} exhibits the same non-monotonic dependence on particle size observed at low temperature for H_C. We wish to stress that the whole series of cobalt ferrite NPs presents K_{eff} values in the same range of stoichiometric bulk $CoFe_2O_4$ ($19x10^6$ erg/cm^3),[60] the largest one being $11.5x10^6$ erg/cm^3 for 20 nm particle size (see table 2). Noteworthy, the estimated K_{eff} values do not exceed the bulk value, as often observed for very small NPs, suggesting that the surface contribution does not significantly modify the effective magnetic anisotropy. In addition, below d_{av} = 20

nm, K_{eff} decreases with the particle size, rather than remaining constant. [53] It is worthwhile to stress that, at least for the smallest samples, the K_{eff} values nicely agree with those evaluated from AC susceptibility measurements (Supporting Information, Fig. SI3)

The temperature evolution of the magnetic properties is better evidenced by plotting H_C and R as a function of normalized temperature, T/T_B (Figure 6a-b). As expected, both H_C and R decay with temperature vanishing for $T = T_B$ However, as concern the R decay, different temperature dependencies are clearly observed: for small NPs, R decays almost linearly meanwhile, for intermediated size (from 10 to 40 nm), it describes a plateau at low temperatures which shifts the linear decay to high T/T_B. Then, for larger NPs (60 nm) a linear decrease similar to that observed for small NPs is restored. On the other hand, H_C always shows a constant decay as a function of T/T_B, although the curvature is not the same for all the family members, being convex for smaller and larger NPs and almost linear for intermediate particle sizes. In addition, the fit of the H_C vs. T/T_B curves using the Stoner-Wohlfarth model provided β factors (Table 2) much larger than that theoretically predicted (0.5 or 0.77), indicating a stronger variation of H_C as a function of the temperature. This discrepancy can be ascribed to the change of the intrinsic magnetic anisotropy upon varying temperature, which so far has not been taken into account, This variation is expected to vary with the particle size and shapes. [61] On the other hand the effect of interparticle interactions can also contribute to the observed behaviour. [41] As a matter fact, both effects are strongly correlated with the trend of K_{eff}: NPs with higher K_{eff} present lower thermal fluctuations as the temperature increases and, thus, different variation of the magnetic anisotropy with the temperature.

In order to quantify the performance as permanent magnets of the family of cobalt ferrite NPs we evaluated the maximum energy product, $(BH)_{max}$, at low and room temperature. $(BH)_{max}$, where B and H are the magnetic induction and the applied field, respectively, is the figure of

merit of permanent magnets and is defined as twice the maximum magnetostatic energy available from a magnet of optimal shape. [62] Figure 7a depicts the room temperature hysteresis loops for 40 nm NPs reported as B or $4\pi M$ vs. H, while the $(BH)_{max}$ values calculated at 5 K and 300K, are shown in Figure 7b. The maximum values we found were 5.4 and 2.1 MGOe (43 and 18 kJ/m^3) at low and RT, respectively. Interestingly, $(BH)_{max}$ shows the same size dependence of K_{eff}, with maxima at 20 nm and 40 nm for low and RT, respectively, confirming the strong relationship existing between the two parameters. It deserves to be noted that, to our knowledge, the $(BH)_{max}$ product found at RT largely exceeds the values previously reported for cobalt ferrite particles (from 0.5 up to 1.1 MGOe) [29,63] although larger H_C were obtained. [29,30] This result can be ascribed to the large magnetic moment of our samples. Indeed, we remind that the $(BH)_{max}$ product increases with H_C only till the coercivity does not exceed $2\pi M_S$. For highly anisotropic material fulfilling the condition $H_C \geq 2\pi M_S$, $(BH)_{max}$ depends only on M_S and R, being the limiting condition $(BH)_{max} \leq (2\pi M_S)^2$. [42,64] In our case, as it is shown in Figure 7a, for 40 nm cobalt ferrite NPs $\mu_0 H_C$ is 3000 G, larger than $2\pi M_S$ (2500 G). Therefore, we can conclude that for coercivities as those commonly observed for cobalt ferrite particles with size in the tenth of nm range, only large M_S, as we obtained in this work, can efficiently increase the $(BH)_{max}$ product. On the other hand, if we assume a complete orientation of the NPs easy axes (i.e. a square hysteresis loops) and bulk density, a magnet obtained by compacting our 40 nm cobalt ferrite NPs, could theoretically reach a $(BH)_{max}$ product of 8 MGOe (60 kJ/m^3). This value largely surpasses the $(BH)_{max}$ of hard magnetic ferrites nowadays commercially available (i.e., 4 MGOe, 30 kJ/m^3). [65] Therefore, cobalt ferrite NPs, such as those reported in the present work, can be realistically considered as a promising material to replace RE-based compounds, at least for all those applications which do not require extraordinarily high magnetic performances.

CONCLUSIONS

In conclusion, we studied the magnetic properties of a family of cobalt ferrite NPs with d_{av} covering a broad range (from 4 to 60 nm), with narrow size distribution and controlled shape and stoichiometry. We found that, while cobalt ferrite NPs present an almost constant values of M_S and M_R, H_C and K_{eff} depict a non-monotonic behaviour with two different maxima at low and RT. We explain the observed behaviour as originating from a combination of cross-over on magnetic coherent/non-coherent rotation and/or demagnetization shape induced effect, which are responsible for the maximum at low temperature, and thermal fluctuations of the blocked moment across the anisotropy energy barrier. Since the latter are more important at lower sizes and higher temperatures, the H_C maximum shifts to larger particle size at RT.

In order to assess the suitability of our cobalt ferrite NPs as permanent magnet, the $(BH)_{max}$ energy product was evaluated. Interestingly, we found the maximum value ever reported in the literature for cobalt ferrite NPs at RT (i.e., 2.1 MGOe (18 MJm^{-3}) for 40 nm NPs). Moreover, this investigation allowed us to establish, at least on the basis of $(BH)_{max}$, the potentiality of cobalt ferrite NPs for the realization of RE free permanent magnet. Indeed, if the possibility of orienting the magnetic anisotropy axes of the nanograins is taken into account, $(BH)_{max}$ as large as 8 MGOe (60 kJ/m3) can be in principle obtained. Furthermore, by playing with the many parameters that define the physical properties of matter at the nanoscale, a further improvement of $(BH)_{max}$ can be envisaged. To this aim several strategies can be considered, such as increasing the particle magnetic moment through the control of the inversion degree of Co ions in the spinel lattice, or by doping with diamagnetic divalent ions. In addition, in order to retain the condition $H_C \geq 2\pi M_S$, the magnetic anisotropy must also be

increased, a task which can be easily realized by modifying the shape and the surface or inducing stresses. On the other hand the NPs described in this work can be also considered as an excellent building block to design exchange coupled systems with enhanced energy product. [66,67] All the above considerations suggest that cobalt ferrite NPs may be a viable alternative to replace RE-based permanent magnet at least in the intermediate region of the energy product map where the latter are currently employed simply because standard ferrites do not have large enough $(BH)_{max}$.

ASSOCIATED CONTENT

M *vs.* T ZFC-FC curves for 4 nm, 7 nm, 11 nm and 20 nm cobalt ferrite NPs; RT hysteresis loops of the family of cobalt ferrite NPs. Temperature dependence of AC susceptibility for 7 nm NPs and Arrhenius plots for 4 nm, 7 nm and 11 nm NPs. Description of data collection and analysis of AC magnetic susceptibility. This material is available free of charge *via* the Internet at http://pubs.acs.org.

AUTHOR INFORMATION

Corresponding Author

*E-mail: lopezortega.alberto@gmail.com, csangregorio@iccom.cnr.it

Note

The authors declare no competing financial interest.

ACKNOWLEDGMENTS

This work is supported by the EU-FP7 NANOPYME Project (No. 310516) and INSTM-Regione Lombardia MAGNANO project. Consorzio GRINT is gratefully acknowledged for providing us access to HIM.

REFERENCES

(1) Goll, D.; Loeffler, R.; Herbst, J.; Karimi, R.; Schneider, G. *J. Phys. Condens. Matter* **2014**, *26* (6), 064208.

(2) Dent, P. C. *J. Appl. Phys.* **2012**, *111* (7), 07A721.

(3) Morrish, A. H. *The Physical Principles of Magnetism*; Willey-VCH, 2001.

(4) Falk, R. B.; Hooper, G. D. *J. Appl. Phys.* **1961**, *32* (3), S190.

(5) Fantechi, E.; Campo, G.; Carta, D.; Corrias, A.; de Julián Fernández, C.; Gatteschi, D.; Innocenti, C.; Pineider, F.; Rugi, F.; Sangregorio, C. *J. Phys. Chem. C* **2012**, *116* (14), 8261–8270.

(6) Bozorth, R.; Tilden, E.; Williams, A. *Phys. Rev.* **1955**, *99* (6), 1788–1798.

(7) Stichauer, L.; Gavoille, G.; Simsa, Z. *J. Appl. Phys.* **1996**, *79* (7), 3645.

(8) Torres, T. E.; Roca, A. G.; Morales, M. P.; Ibarra, A.; Marquina, C.; Ibarra, M. R.; Goya, G. F. *J. Phys. Conf. Ser.* **2010**, *200* (7), 072101.

(9) Fantechi, E.; Innocenti, C.; Zanardelli, M.; Fittipaldi, M.; Falvo, E.; Carbo, M.; Shullani, V.; Di Cesare Mannelli, L.; Ghelardini, C.; Ferretti, A. M.; Ponti, A.; Sangregorio, C.; Ceci, P. *ACS Nano* **2014**, *8* (5), 4705–4719.

(10) Lee, J.-H.; Huh, Y.-M.; Jun, Y.; Seo, J.; Jang, J.; Song, H.-T.; Kim, S.; Cho, E.-J.; Yoon, H.-G.; Suh, J.-S.; Cheon, J. *Nat. Med.* **2007**, *13* (1), 95–99.

(11) Shinde, A. B. *Int. J. Innov. Technol. Explor. Eng.* **2013**, *3* (4), 64–67.

(12) Sugimoto, M. *J. Am. Ceram. Soc.* **2004**, *82* (2), 269–280.

(13) Carey, M. J.; Maat, S.; Rice, P.; Farrow, R. F. C.; Marks, R. F.; Kellock, A.; Nguyen, P.; Gurney, B. A. *Appl. Phys. Lett.* **2002**, *81* (6), 1044.

(14) Xiong, P.; Huang, H.; Wang, X. *J. Power Sources* **2014**, *245*, 937–946.

(15) Rajput, J. K.; Kaur, G. *Catal. Sci. Technol.* **2014**, *4* (1), 142–151.

(16) Khatkhatay, F. *IEEE Trans. Appl. Supercond.* **2013**, *23* (3), 8001204–8001204.

(17) Chen, D.; Yi, X.; Chen, Z.; Zhang, Y.; Chen, B.; Kang, Z. *Int. J. Appl. Ceram. Technol.* **2013**, *11* (5), 954–959.

(18) Khedr, M. H.; Omar, A. A.; Abdel-Moaty, S. A. *Colloids Surfaces A Physicochem. Eng. Asp.* **2006**, *281* (1-3), 8–14.

(19) Song, Q.; Zhang, Z. J. *J. Am. Chem. Soc.* **2004**, *126* (19), 6164–6168.

(20) Chinnasamy, C. N.; Jeyadevan, B.; Shinoda, K.; Tohji, K.; Djayaprawira, D. J.; Takahashi, M.; Joseyphus, R. J.; Narayanasamy, A. *Appl. Phys. Lett.* **2003**, *83* (14), 2862.

(21) Sun, S.; Zeng, H.; Robinson, D. B.; Raoux, S.; Rice, P. M.; Wang, S. X.; Li, G. *J. Am. Chem. Soc.* **2004**, *126* (1), 273–279.

(22) Cozzoli, D. *Advanced Wet-Chemical Synthetic Approaches to Inorganic Nanostructures*; Cozzoli, P. D., Ed.; Transworld Research Network, 2008.

(23) Salazar-Alvarez, G.; Olsson, R. T.; Sort, J.; Macedo, W. A. A.; Ardisson, J. D.; Baró, M. D.; Gedde, U. W.; Nogués, J. *Chem. Mater.* **2007**, *19* (20), 4957–4963.

(24) Jian, G.; Fu, Q.; Zhou, D. *J. Magn. Magn. Mater.* **2012**, *324* (5), 671–676.

(25) Liu, C.; Zou, B.; Rondinone, A. J.; Zhang, Z. J. *J. Am. Chem. Soc.* **2000**, *122* (26), 6263–6267.

(26) Maaz, K.; Mumtaz, A.; Hasanain, S. K.; Ceylan, A. *J. Magn. Magn. Mater.* **2007**, *308* (2), 289–295.

(27) Bao, N.; Shen, L.; Padhan, P.; Gupta, A. *Appl. Phys. Lett.* **2008**, *92* (17), 173101.

(28) Bao, N.; Shen, L.; An, W.; Padhan, P.; Heath Turner, C.; Gupta, A. *Chem. Mater.* **2009**, *21* (14), 3458–3468.

(29) Ponce, A. S.; Chagas, E. F.; Prado, R. J.; Fernandes, C. H. M.; Terezo, A. J.; Baggio-Saitovitch, E. *J. Magn. Magn. Mater.* **2013**, *344* (Complete), 182–187.

(30) Liu, B. H.; Ding, J. *Appl. Phys. Lett.* **2006**, *88* (4), 042506.

(31) Seo, W. S.; Jo, H. H.; Lee, K.; Kim, B.; Oh, S. J.; Park, J. T. *Angew. Chem. Int. Ed. Engl.* **2004**, *43* (9), 1115–1117.

(32) Lutterotti, L. MAUD program http://www.ing.unitn.it/~maud/.

(33) Rietveld, H. M. *J. Appl. Crystallogr.* **1969**, *2*, 65–71.

(34) Tachiki, M. *Prog. Theor. Phys.* **1960**, *23* (6), 1055–1072.

(35) Lopes-Moriyama, A. L.; Madigou, V.; Souza, C. P. de; Leroux, C. *Powder Technol.* **2014**, *256*, 482–489.

(36) Wang, Z. L.; Feng, X. *J. Phys. Chem. B* **2003**, *107* (49), 13563–13566.

(37) Cammarata, R.; Sieradzki, K. *Phys. Rev. Lett.* **1989**, *62* (17), 2005–2008.

(38) Kneller, E. F.; Luborsky, F. E. *J. Appl. Phys.* **1963**, *34* (3), 656.

(39) Bean, C. P.; Livingston, J. D. *J. Appl. Phys.* **1959**, *30* (4), S120.

(40) García-Otero, J.; García-Bastida, A. J.; Rivas, J. *J. Magn. Magn. Mater.* **1998**, *189* (3), 377–383.

(41) Knobel, M.; Nunes, W. C.; Socolovsky, L. M.; De Biasi, E.; Vargas, J. M.; Denardin, J. C. *J. Nanosci. Nanotechnol.* **2008**, *8*, 2836–2857.

(42) Cullity, B. D.; Graham, C. D. *Introduction to Magnetic Materials, 2nd Edition*; Wiley-IEEE Press, 2008.

(43) Fonseca, F.; Goya, G.; Jardim, R.; Muccillo, R.; Carreño, N.; Longo, E.; Leite, E. *Phys. Rev. B* **2002**, *66* (10), 104406.

(44) Salazar-Alvarez, G.; Qin, J.; Sepelák, V.; Bergmann, I.; Vasilakaki, M.; Trohidou, K. N.; Ardisson, J. D.; Macedo, W. A. A.; Mikhaylova, M.; Muhammed, M.; Baró, M. D.; Nogués, J. *J. Am. Chem. Soc.* **2008**, *130* (40), 13234–13239.

(45) Brown, W. F. *Ann. N. Y. Acad. Sci.* **1969**, *147* (12), 463–488.

(46) Guimarães, A. P. *Principles of Nanomagnetism*; Springer Berlin Heidelberg: Berlin, Heidelberg, 2009.

(47) Rafique, M. Y.; Pan, L.; Javed, Q.; Iqbal, M. Z.; Yang, L. *J. Nanoparticle Res.* **2012**, *14* (10), 1189.

(48) Okamoto, S.; Kitakami, O.; Kikuchi, N.; Miyazaki, T.; Shimada, Y.; Takahashi, Y. *Phys. Rev. B* **2003**, *67* (9), 094422.

(49) Skomski, R. *J. Phys. Condens. Matter* **2003**, *15* (20), R841.

(50) Wang, J.; Zhao, F.; Wu, W.; Cao, S.-H.; Zhao, G. *Phys. Lett. A* **2012**, *376* (4), 547–549.

(51) Chinnasamy, C. N.; Jeyadevan, B.; Perales-Perez, O.; Shinoda, K.; Tohji, K.; Kasuya, A. *IEEE Trans. Magn.* **2002**, *38* (5), 2640–2642.

(52) Maaz, K.; Mumtaz, A.; Hasanain, S. K.; Bertino, M. F. *J. Magn. Magn. Mater.* **2010**, *322* (15), 2199–2202.

(53) Stoner, E. C.; Wohlfarth, E. P. *Philos. Trans. R. Soc. A Math. Phys. Eng. Sci.* **1948**, *240* (826), 599–642.

(54) Soshin Chikazumi. In *Physics of Ferromagnetism*; Oxford University Press: New York,USA, 2009; pp 537–580.

(55) Kodama, R. . *J. Magn. Magn. Mater.* **1999**, *200* (1-3), 359–372.

(56) Moumen, N.; Bonville, P.; Pileni, M. P. *J. Phys. Chem.* **1996**, *100* (34), 14410–14416.

(57) Usov, N. A.; Peschany, S. E. *J. Magn. Magn. Mater.* **1997**, *174* (3), 247–260.

(58) García-Otero, J.; Porto, M.; Rivas, J.; Bunde, A. *J. Magn. Magn. Mater.* **1999**, *203* (1-3), 268–270.

(59) Dormann, J.; D'Orazio, F.; Lucari, F.; Tronc, E.; Prené, P.; Jolivet, J.; Fiorani, D.; Cherkaoui, R.; Noguès, M. *Phys. Rev. B* **1996**, *53* (21), 14291–14297.

(60) Shenker, H. *Phys. Rev.* **1957**, *107* (5), 1246–1249.

(61) De Julián Fernández, C. *Phys. Rev. B* **2005**, *72* (5), 054438.

(62) Coey, J. M. D. Hard Magnetic Materials: A Perspective. *Magnetics, IEEE Transactions on*, 2011, *47*, 4671–4681.

(63) De Assis Olimpio Cabral, F.; de Araujo Machado, F. L.; de Araujo, J. H.; Soares, J. M.; Rodrigues, A. R.; Araujo, A. *IEEE Trans. Magn.* **2008**, *44* (11), 4235–4238.

(64) Fullerton, E. E.; Jiang, J. .; Bader, S. . *J. Magn. Magn. Mater.* **1999**, *200* (1-3), 392–404.

(65) Gutfleisch, O.; Willard, M. A.; Brück, E.; Chen, C. H.; Sankar, S. G.; Liu, J. P. *Adv. Mater.* **2011**, *23* (7), 821–842.

(66) Soares, J. M.; Cabral, F. A. O.; de Araújo, J. H.; Machado, F. L. A. *Appl. Phys. Lett.* **2011**, *98* (7), 072502.

(67) López-Ortega, A.; Estrader, M.; Salazar-Alvarez, G.; Roca, A. G.; Nogués, J. *Phys. Rep.* **2015**, *553*, 1–32.

Table1. Summary of the synthesis parameters and structural data obtained from TEM, XRD and XRF analysis (in the latter case x refers to the Co content per formula unit, $Co_xFe_{3-x}O_4$). TEM particle size has been assessed by taking into account the diameter for spherical NPs (d) and the edge length for cubes or octahedrons (l).

	Cobalt precursor	Surfactants	Decomposition temperature (ºC)	Digestion time (min)	Heating rate (º/min)	TEM size (nm)	XRF (x)	XRD size (nm)	Cell parameter (nm)
1	$Co(acac)_2$	ONH_2	210	300	Fast	4(1) [d]	0.7	4	0.839(1)
2	$Co(acac)_2$	OA/ ONH_2	300	30	3	7(1) [d]	0.7	8.8	0.398(1)
3	$Co(acac)_2$	OA/ ONH_2	300	60	3	11(1) [d]	0.7	16	0.840(1)
4	$CoCl_2$	OA/ ONH_2	270	15	3	20(2) [l]	0.6	30	0.842(1)
5	$CoCl_2$	OA/ ONH_2	270	60	3	30(4) [l]	0.7	35	0.840(1)
6	$CoCl_2$	OA/ ONH_2	270	15	1	40(7) [l]	0.6	50	0.841(1)
7	$CoCl_2$	OA/ ONH_2	270	60	1	60(4) [l]	0.6	80	0.840(1)

Table 2. Magnetic properties of cobalt ferrite NPs

TEM size (nm)	T_B exp. (K)	T_B calc. (K)	H_C (5K) (kOe)	M_S (5K) (emu/g)	R (5K) (M_S/M_R)	H_C (0) (kOe)	β	Keff (10^6 erg/cm^3)
4(1) [d]	90	110	11.0	59.4	0.51	12.7	3.3	6.0
7(1) [d]	220	200	13.5	77.4	0.76	14.0	1.9	8.5
11(1) [d]	300	310	14.7	80.0	0.76	15.5	1.8	9.7
20(2) [l]	----	430	16.7	85.5	0.83	17.4	2.0	11.6
30(4) [l]	----	480	12.1	89.1	0.77	12.5	2.0	8.7
40(7) [l]	----	540	10.0	88.7	0.77	10.2	1.5	7.0
60(4) [l]	----	620	0.8	84.7	0.74	8.3	1.4	5.0

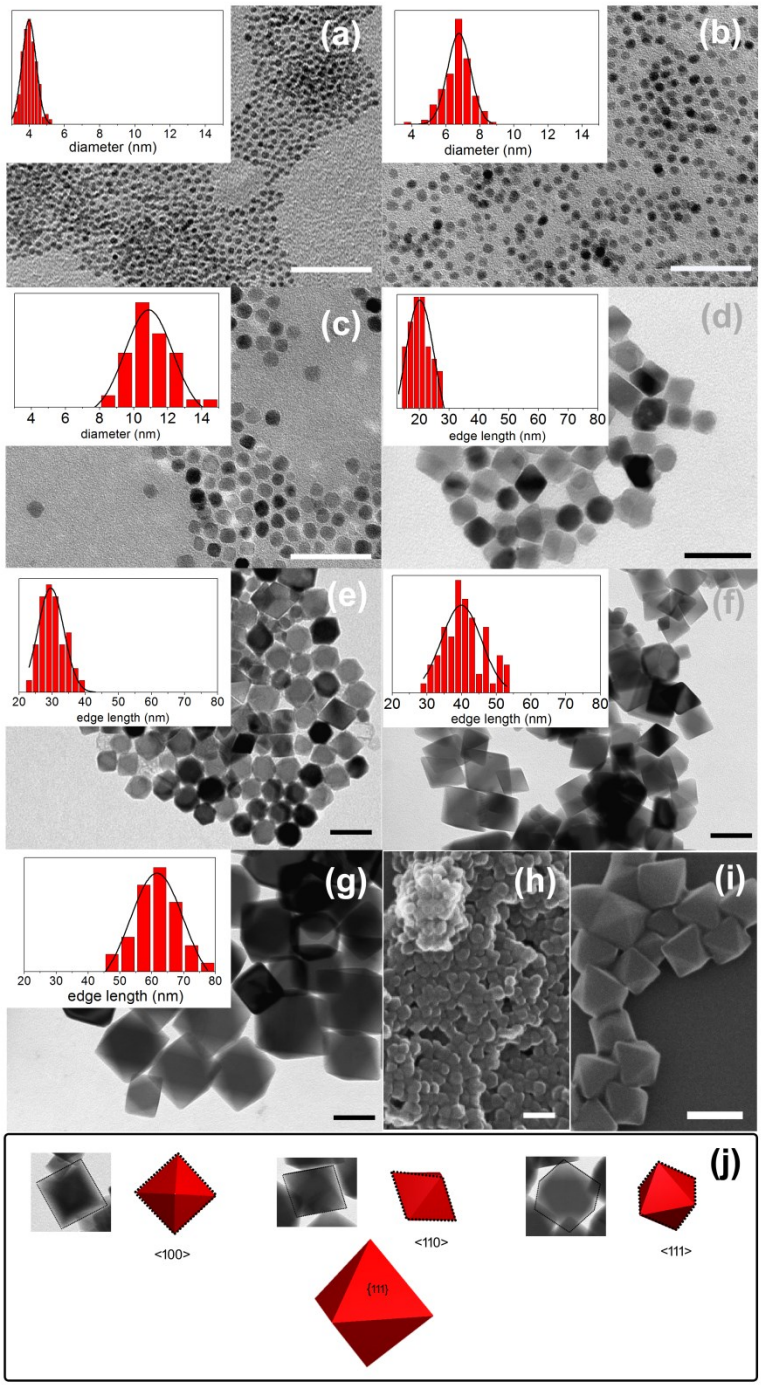

Figure 1. TEM images and particle size histograms for NPs of (a) 4, (b) 7, (c) 11, (d) 20, (e) 30, (f) 40 and (g) 60 nm (scale bars correspond to 50 nm); HIM images for (h) 20 and (i) 40 nm NPs, respectively (scale bars correspond to 100 nm); and (j) 2D TEM projections for octahedral NPs.

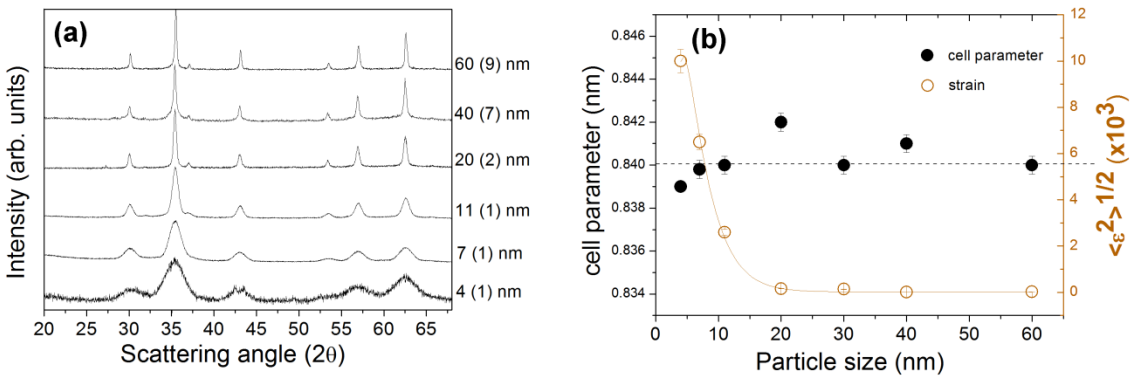

Figure 2. (a) XRD patterns for the series of cobalt ferrite NPs and (b) cell parameter (left scale) and microstrain (right scale) dependence on particle size.

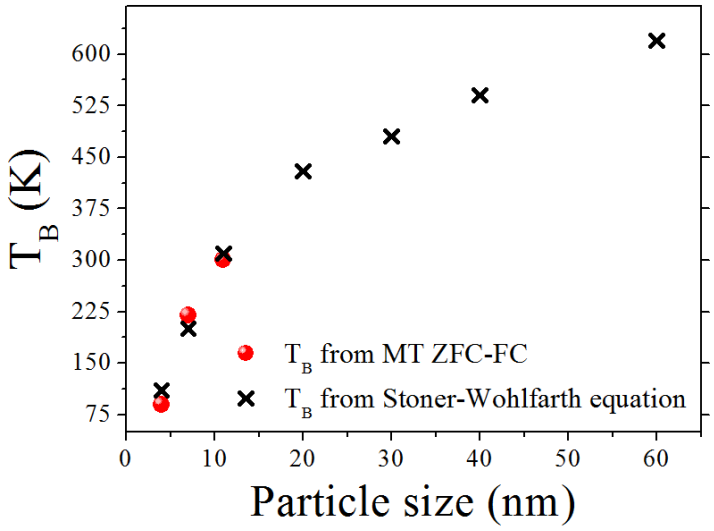

Figure 3. Size dependence of the blocking temperatures; T_B were obtained by M *vs.* T ZFC-FC measurements (red spheres) or by fitting H_C *vs.* T curves to the Stoner-Wohlfarth equation, $H_C=H_C(0)[1-(T/T_B)]^{\beta}$ (black crosses).

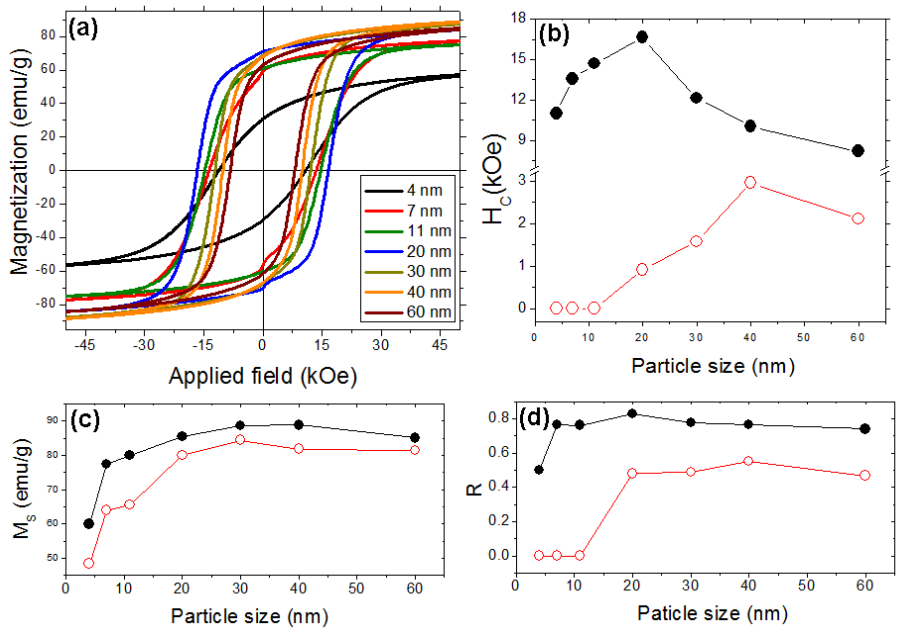

Figure 4. (a) Low temperature (5 K) hysteresis loops of the family of cobalt ferrite NPs; (b,c and d) size dependence of H_C, M_S and R measured at 5 K (full black dots) and 300 K (empty red dots).

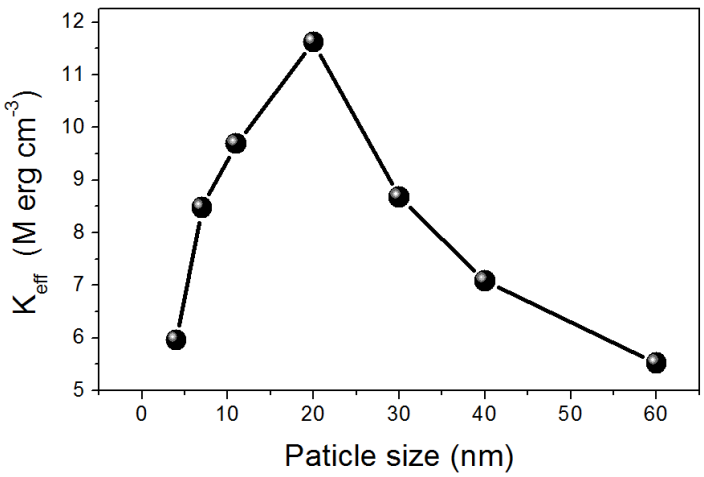

Figure 5. Effective magnetic anisotropy, K_{eff}, of cobalt ferrite NPs with different particle sizes. The data were obtained from hysteresis loops at variable temperatures neglecting any temperature-dependent term and assuming only coherent rotation switching mode.

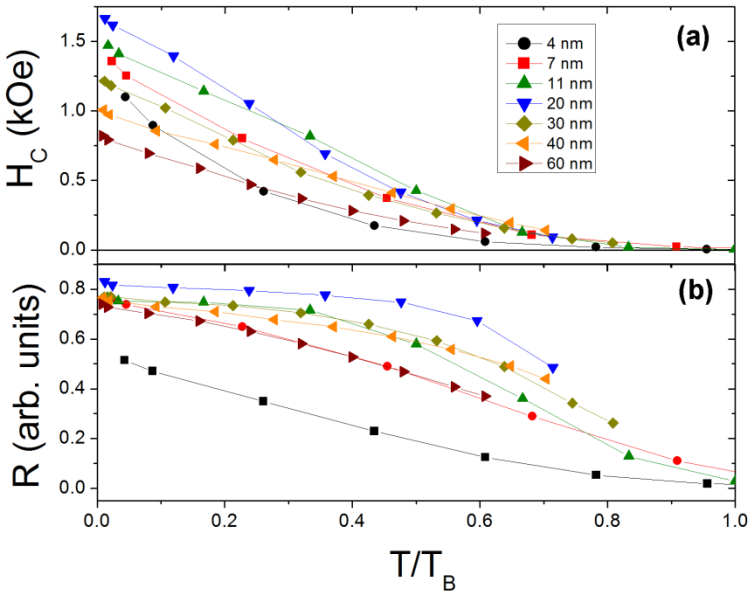

Figure 6. Evolution of (a) H_C and (b) R for the series of cobalt ferrite NPs as a function of T/T_B.

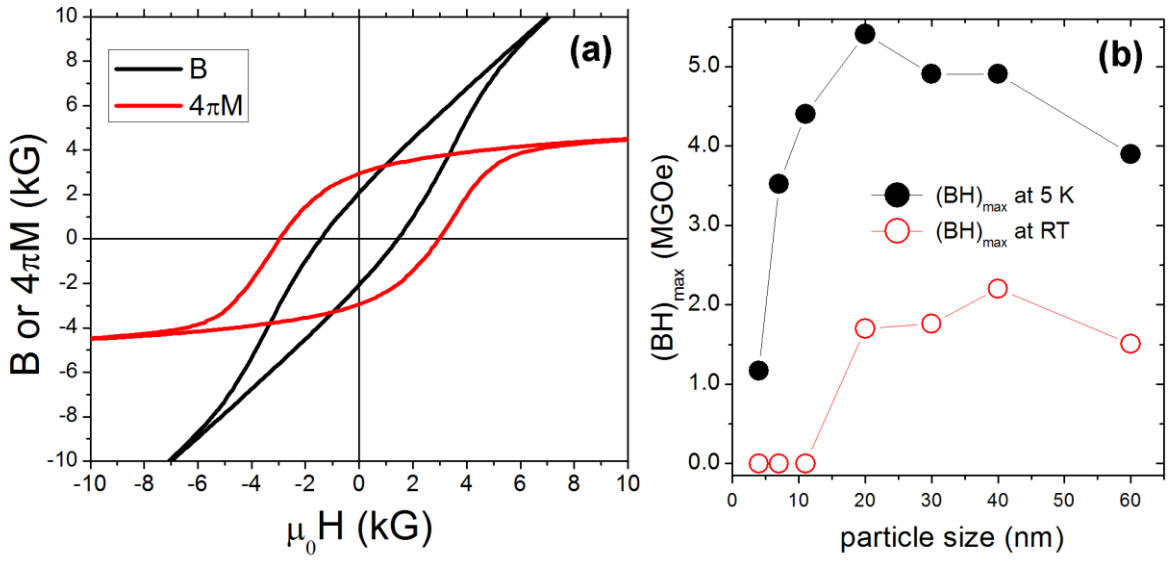

Figure 7. (a) B and 4πM vs. H loops for 40 nm NPs at RT and (b) $(BH)_{max}$ at 5K (black solid circles) and RT (red empty circles) as a function of the particle size.

TOC

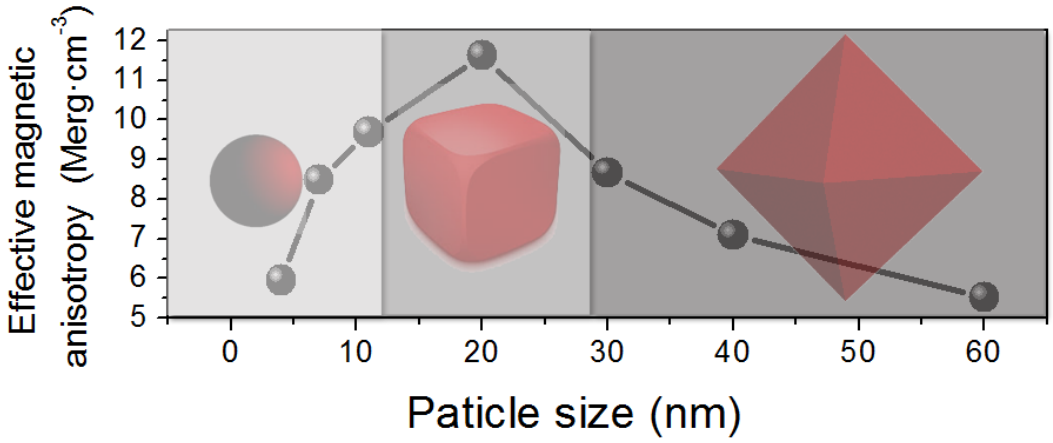
Effective magnetic anisotropy (Merg·cm-3)
12
11
10
9
8
7
6
5
0
10
20
30
40
50
60
Paticle size (nm)